Available online at www.sciencedirect.com
ScienceDirect
Journal of the European Ceramic Society 29 (2009) 653–659
www.elsevier.com/locate/jeurceramsoc

Porous stabilized zirconia coatings on zircon using volatility diagrams

P. Barreiro *, P. Rey [1], A. Souto [2], F. Guitián

Instituto de Cerámica de Galicia, Mestre Mateo s/n, Campus Sur-Universidade, 15782 Santiago de Compostela, Spain

Received 8 May 2008; received in revised form 8 July 2008; accepted 9 July 2008
Available online 2 September 2008

Abstract

A process for obtaining porous coatings of yttria stabilized zirconia on zircon substrates is described. The calcination in reducing atmospheres (oxygen partial pressures below 2×10^{-9} atm and at temperatures over 1300 °C) of test samples containing zircon and small amounts of yttria led to the formation of porous stabilized zirconia coatings (up to 240 μm thick) on the samples. The process led to the decomposition of the silica contained in the zircon, volatilized in the form of $SiO_{(gas)}$, originating pores in its place. The conditions required for the process were inferred from the volatility diagrams of the involved chemical species, which were likewise used to analyze the experimental results.

Keywords: Calcination; Powder–gas phase reaction; Porosity; Silicate; Volatility diagrams

1. Introduction

The coating process on monolithic ceramics results in a composite material with features that could not be easily achieved with the coating or substrate materials on their own, combining their properties, and reducing costs.

Zirconia (ZrO_2) is a refractory ceramic showing a high melting point and resistance to chemical attacks. Being hard and friction resistant, it is used for improving the quality and extending the lifespan of cutting parts, gears or extrusion dies.

Phase transformations are the main limitation on the use of zirconia as a technical material, as zirconia exhibits three well-defined polymorphs[1]: monoclinic (stable up to 1170 °C), tetragonal (up to 2370 °C) and cubic (up to the melting point of 2680 °C), and also a high pressure orthorhombic form exists. With increasing temperature, phase changes, and the subsequent changes in volume, can cause cracking or a catastrophic failure in zirconia pieces. This is solved in technical ceramics by means of the addition of oxides, such as CaO, MgO or Y_2O_3, which, in the right proportion, stabilize zirconia in tetragonal or cubic form.[1]

Zircon ($ZrSiO_4$) has as well a high melting point and resistance to chemically aggressive atmospheres, although not as much as zirconia. As it does not undergo any phase transformation, its resistance to high temperatures and thermal shock is very high. Although the properties of zircon are not as outstanding as those of zirconia, it is a much more affordable material and more readily available, being therefore very used as a refractory.[2]

Stabilized zirconia and zircon composites offer the excellent thermal and mechanical properties of stabilized zirconia, whilst the parts not subjected to high requirements are made of more affordable zircon.

Thin and porous layers of stabilized zirconia are usually made by the inclusion of pore forming particles, such as graphite or polymer particles. Those particles are thermally eliminated during or before the sintering. There are different coating methods, from chemical vapour deposition (CVD)[3] and plasma spraying[4] to impregnation and sol–gel processes.[5]

A new processing route for porous stabilized zirconia coatings on zircon substrates is presented. This process consists in the transformation of the surface layer of a zircon ceramic into porous zirconia by heating the ceramic at high temperature in a controlled reducing atmosphere. Under appropriate conditions[6] the SiO_2 contained in zircon is selectively reduced and volatilized from the ceramic surface in the form of $SiO_{(g)}$, leaving a porous surface layer of zirconia. This coating process can be carried out on sintered zircon or simultaneously to the sintering. The stabilization of the zirconia coating in tetragonal

* Corresponding author. Tel.: +34 981 563100x16875.
E-mail address: pablo.barreiro@usc.es (P. Barreiro).
[1] Present address: AIMEN, C/Relva, 27A, Torneiros, 36410 Porriño, Spain.
[2] Present address: Ferroatlántica I + D, Sabón, 15142 Arteixo, Spain.

0955-2219/$ – see front matter © 2008 Elsevier Ltd. All rights reserved.
doi:10.1016/j.jeurceramsoc.2008.07.018

or cubic phase is possible through the addition of a stabilizing oxide (Y_2O_3 in this case) to the zircon prior to the sintering.

The fact of the coating being generated directly from the substrate increases continuity in the coating–substrate interface, and it also makes unnecessary the use of complex coating methods, resulting very useful for extremely thin layers.

The conditions required for the process were inferred from the volatility diagrams of the involved chemical species. These diagrams were also used for the interpretation of the experimental results.

Volatility diagrams are isothermal plots of equilibrium thermochemical data, and show the partial pressures of gaseous species in equilibrium with the condensed phases (liquid or solid) in a system. In the present article, volatility diagrams are built and used according to the methodology of Lou et. al.,[7] and using the same concepts (isomolar and isobaric lines, etc.).

The use of volatility diagrams in the production of porous structures through selective volatilization of one of the components of the system has been reported in previous publications.[8,9] In an analogous way, silica volatilization at high temperatures takes place in other silica-containing materials as well, such as mullite.[10] The process can be extended to those materials.

2. Experimental procedure

The starting materials were zircon ($ZrSiO_4$ M5, ALMIBERIA S.A., Spain), with a particle size of 1.8 μm (measured with a particle size analyzer, Model Sedigraph 5100, Micromeritics Instrument Corp., Norcross, GA, USA) and a purity of 95% (determined by inductively coupled plasma-atomic emission spectrometry (ICP-AES) in a Varian Liberty 200, Melbourne, Australia: SiO_2: 33.5; ZrO_2: 61.5; HfO_2: 2.0; $Al_2O_3 < 1$; $TiO_2 < 0.3$; $Fe_2O_3 < 0.15$) and yttria (Y_2O_3, Goodfellow Cambridge Ltd., 99.9% of purity and an average particle size of 1 μm). The powders were milled in an attrition grinder for 1 h to obtain a homogeneous mixture. The amount of yttria used is an 8 mol% of the zircon–yttria mixture (corresponding to 8 mol% of the zirconia–yttria mixture).

Discs (12.5 mm diameter and 1 mm thick) were made using the powder mixture, through cold uniaxial pressing at 560 MPa (Model 15.011 Graseby-Specac, Kent, UK). These discs were sintered in an electric furnace (Lenton UAF 16/5) at 1400 °C for 2 h (heating and cooling rate of 5 °C/min).

The $ZrSiO_4/Y_2O_3$ discs were then placed on Al_2O_3 crucibles and loaded into a graphite-lined furnace (Model HI-16L/17, Pyrox Technologies, Rambouillet, France), equipped with W5%Re–W26%Re thermocouples and a gas control system, including a vacuum pump and an Pirani gauge for measuring the internal pressure.

Once the furnace was loaded and closed, in order to purge the oxygen in the furnace, the pressure inside was pumped down to 10^{-3} atm. It was then filled to atmospheric pressure with nitrogen (Air Liquide N_2 1; $P_{O_2} < 2 \times 10^{-6}$ atm). This process was carried out again, and later the pressure was pumped down for a third time without filling the furnace with nitrogen. This way, the total pressure in the furnace was 10^{-3} atm and the oxygen partial pressure was $P_{O_2} < 2 \times 10^{-9}$ atm.

At this point, the heating was begun, with a heating rate of 5 °C/min. Once reached a certain temperature (1300 or 1400 °C), the temperature was kept constant for a time between 1 and 4 h, being the furnace afterwards cooled to room temperature at a 5 °C/min rate. The vacuum pump was operated throughout the whole process to ensure the constant total pressure of 10^{-3} atm.

Assuming a complete reaction between the remaining O_2 and the graphite furnace lining at the working temperatures, by the time the reaction temperature was reached the value of P_{CO} would have been $<4 \times 10^{-9}$ atm.

The process was also carried out with different number of gas purges, from 0 to 3 times. If the furnace is not purged, a higher amount of oxygen is left, reacting with the graphite elements in the furnace. Assuming all the oxygen reacts to produce CO, the maximal initial pressure of CO would be 4×10^{-4} atm (non-purged), 4×10^{-7} atm (purged 1 time) and 4×10^{-9} atm (purged 2 or 3 times).

The weight variations due to the process were determined on an analytical balance (Mettler AE200, Greifensee, Switzerland), with an accuracy of ±0.1 mg. The identification of the crystalline phases was carried out with X-ray diffraction (XRD, Model D5000 Siemens, Karlsruhe, Germany) using Cu Kα radiation at 30 Ma–40 kV, with scanning speed of $1° \text{ min}^{-1}$ ($0.0250° \text{ step}^{-1}$). The thickness and microstructure of the coatings made were studied with a scanning electron microscope (SEM, Model JSM-6400, JEOL, Tokyo, Japan) coupled to a energy dispersive spectroscopy microprobe (EDS, INCA Oxford Instruments, Buckinghamshire, UK). The initial porosity of the samples and that developed after the thermal treatments were measured by mercury intrusion porosimetry (Model Autopore II 9215, Micromeritics).

Volatility diagrams used in this work were built following the methodology of Lou et al.[7] using thermodynamic data obtained from the program FACTSAGE.[11]

3. Results

The zircon/yttria test samples underwent a superficial volatilization due to a thermal process at high temperatures and low oxygen partial pressure, resulting in the formation of a porous yttria stabilized zirconia coating. Fig. 1A shows an SEM micrography of the polished facture surface of one of the discs, heated under vacuum for 4 h at 1300 °C. Fig. 1B shows another test sample subjected to a similar thermal treatment at 1400 °C. A highly porous surface layer is formed on both samples. As an example, Fig. 1C shows in more detail the core of the disc depicted in Fig. 1C, whilst Fig. 1D shows the porous layer generated on it. The sample calcined at 1300 °C has a 60 μm thick porous layer, whilst that calcined at 1400 °C has a layer exceeding 240 μm in thickness.

Fig. 2A shows the SEM micrography of the fracture surface of a zircon sample, calcined at 1400 °C for 1 h, on which a porous layer of about 100 μm thickness is formed. Figs. 2B–D show the corresponding EDS maps for the elements Si, Zr and Y. The EDS maps reveal the presence of silicon in the dense part of the piece, but not in the porous layer. On the other hand, zirconia

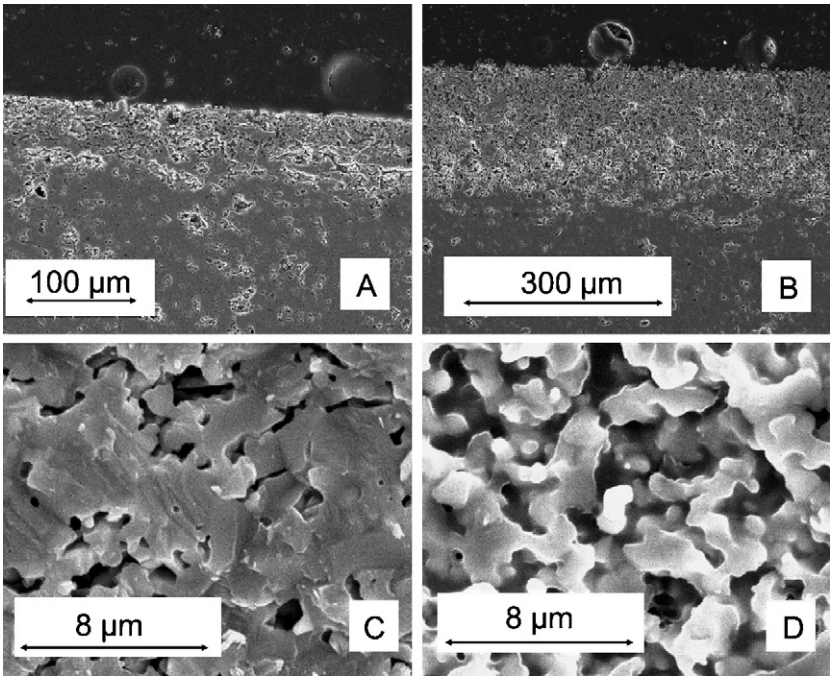

Fig. 1. Zircon test samples heated under vacuum for 4 h at (A) 1300 °C and (B) 1400 °C. Closer views depict the core of the second sample (C) and the porous layer (D).

and yttria are present both in the dense part of the disc and the porous outer layer.

XRD analysis showed the only crystalline phase on the porous layer is stabilized zirconia. Fig. 3 shows the diffractogram of the starting powder (zircon and yttria), prior to sintering, and the diffractogram of the same disc after being sintered and calcined under vacuum at 1400 °C for 4 h. In the first XRD diffractogram both yttria and zircon are found, whilst on the calcined sample the peaks found are those corresponding to stabilized zirconia and residual presence of zircon. In the interval of 2θ between 50° and 80°, where cubic and tetragonal zirconia have different XRD patterns the characteristic peaks of cubic zirconia are the most relevant, but some less relevant peaks corresponding to tetragonal zirconia are also seen (as shoulders in the main peaks), meaning that the yttria stabilized zirconia porous layer presents both polymorphs, tetragonal and cubic, the latter being predominant.

Porosity has been determined by means of mercury intrusion porosimetry analysis (Fig. 4). The porosity of the samples increased with their thermal treating, due to the formation of the outer layer, having the generated porosity a homogeneous distribution of pore sizes, with most generated pores ranging between 1 and 3 μm in diameter.

Fig. 5 shows the weight loss of the test samples after different reaction times, at 1300 and 1400 °C. Weight losses are higher for longer reaction times, decreasing the loss rate gradually with time. The samples calcined at higher temperature show

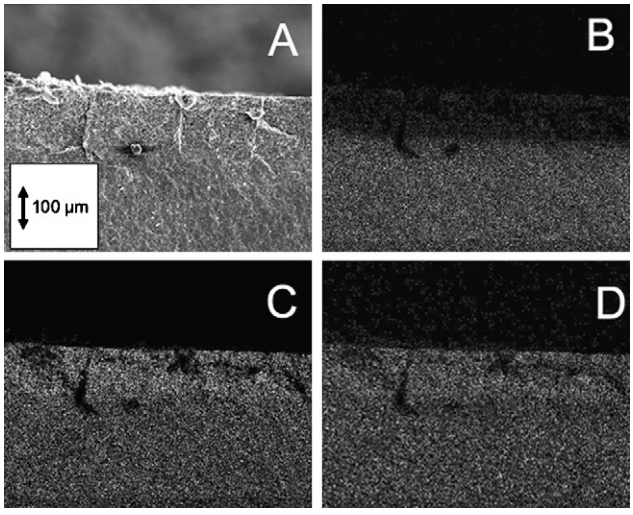

Fig. 2. SEM micrograph of the fracture surface of a zircon test sample, heated under vacuum at 1400 °C for 1 h (A) and corresponding EDS maps for Si (B), Zr (C) and Y (D).

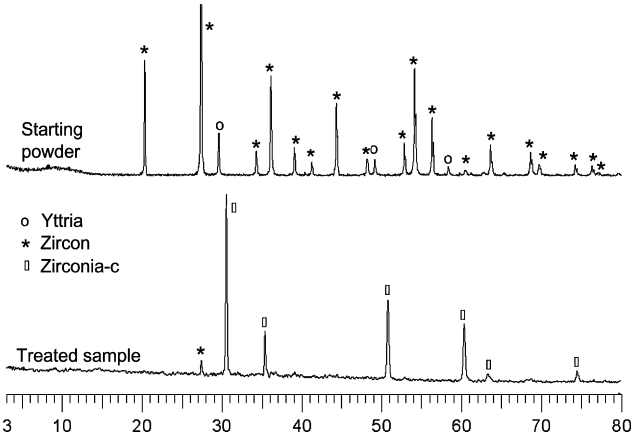

Fig. 3. Diffractograms of a test sample calcined at 1400 °C for 4 h in vacuum (lower) and the starting power (upper).

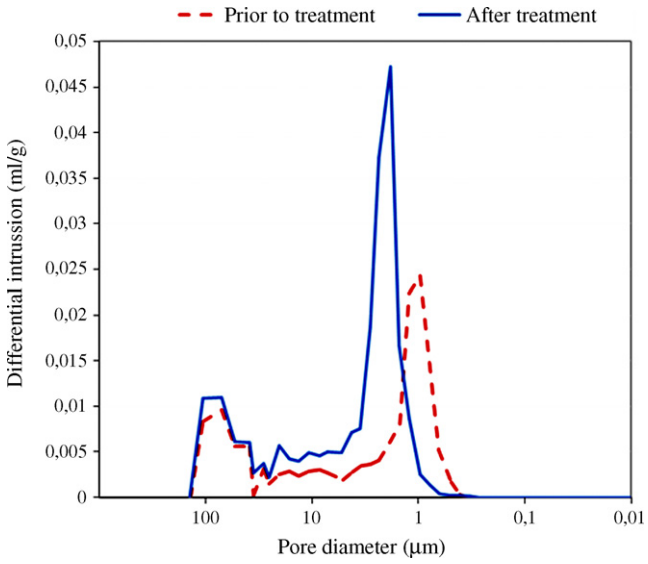

Fig. 4. Mercury intrusion porosimetry analysis of zircon discs before and after thermal processing in reducing atmosphere (1400 °C/4 h).

the highest weight losses, up to 12.5% of the original weight after 4 h.

Fig. 6 shows weight losses for a test sample for 120 min reaction time at 1400 °C, for different number of previous purges of the furnace atmosphere. Weight losses are higher if the furnace is purged less times, that is, when the content of CO in the atmosphere is higher.

4. Discussion

The formation of stabilized zirconia coatings on zircon ceramics is due to the selective volatilization of silica when zircon ceramics are thermally treated in reducing atmospheres at high temperatures.

The results of the experiments are explained by the relative stabilities of the oxides into which zircon decomposes under high temperature and reducing conditions (ZrO_2 and SiO_2). The volatilization and equilibrium can be studied by means of volatility diagrams. Fig. 7 shows the $ZrSiO_4$ volatility diagram and

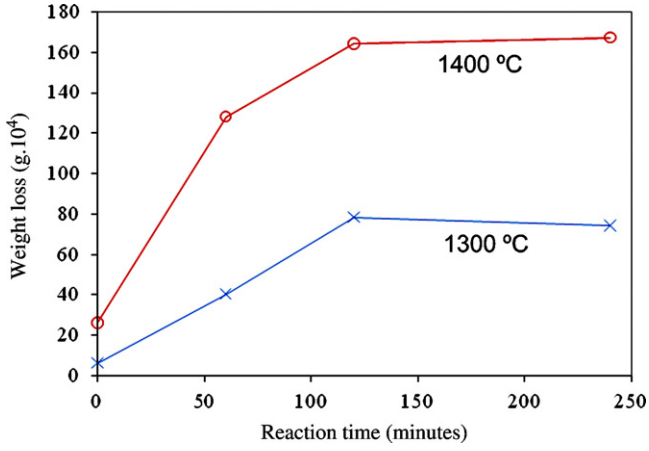

Fig. 5. Mass loss for zircon test samples variation with time at different temperatures.

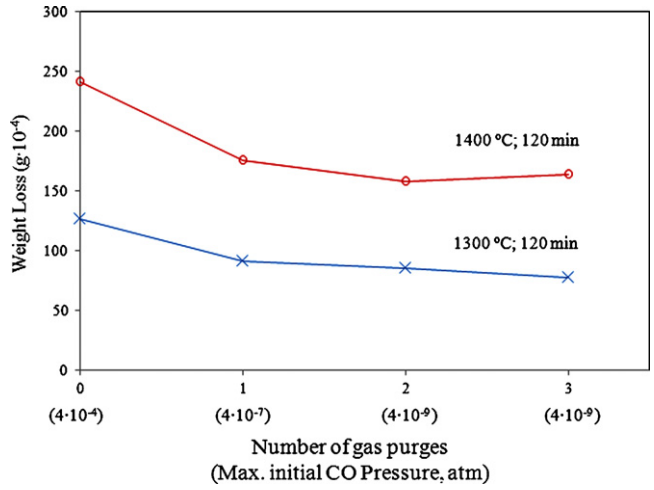

Fig. 6. Mass loss for zircon test samples after 120 min at different temperatures for different number of gas purges in the furnace.

Table 1 shows the reactions used in its construction at 1400 °C. According to the diagram, the reaction that takes place in the volatilization process is the following:

$$ZrSiO_4 + Y_2O_3 \rightarrow ZrO_2 + Y_2O_3 + SiO_{(g)} + \tfrac{1}{2}O_{2(g)} \quad (1)$$

The porosimetry analysis (Fig. 4) showed how the porosity of the samples increased after the thermal treatment in reducing conditions and how the pores increased in size. This is explained by the volatilization mechanism: the reaction takes place on the

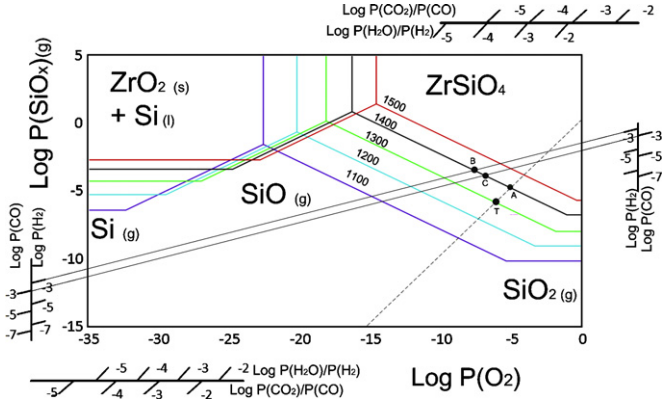

Fig. 7. Volatility diagram for zircon under a total pressure of 10^{-3} atm and different temperatures.

Table 1
Reactions used in the construction of the volatility diagrams of $ZrSiO_4$ and values of the equilibrium constant at 1400 °C and 10^{-3} atm total pressure

Reactions used	K_{eq} (1400 °C, 10^{-3} atm)
$ZrSiO_{4(s)} \rightarrow ZrO_{2(s)} + SiO_{(g)} + \frac{1}{2}O_{2(g)}$	5.56×10^{-8}
$ZrSiO_{4(s)} \rightarrow ZrO_{2(s)} + Si_{(l)} + O_{2(g)}$	5.26×10^{-17}
$ZrSiO_{4(s)} \rightarrow ZrO_{2(s)} + SiO_{2(g)}$	1.76×10^{-7}
$Si_{(l)} \rightarrow Si_{(g)}$	4.21×10^{-4}
$Si_{(l)} + \frac{1}{2}O_{2(g)} \rightarrow SiO_{(g)}$	$1.06 \times 10^{+9}$
$ZrSiO_{4(s)} + H_{2(g)} \rightarrow ZrO_{2(s)} + SiO_{(g)} + H_2O_{(g)}$	1.17×10^{-4}
$ZrSiO_{4(s)} + CO_{(g)} \rightarrow ZrO_{2(s)} + SiO_{(g)} + CO_{2(g)}$	3.60×10^{-5}

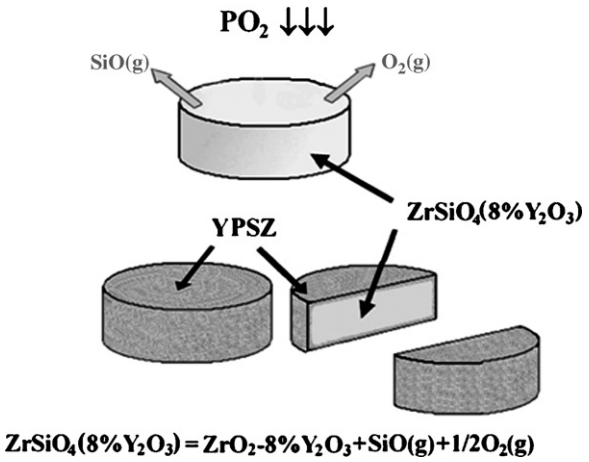

Fig. 8. Schematic representation of the silica volatilization of zircon/yttria samples.

exposed surfaces, producing pores and increasing the size of the already existing pores.

According to the zircon volatility diagram, the equilibrium conditions for this reaction at 1400 °C and 10^{-3} atm are $P_{SIO} = 1.8 \times 10^{-5}$ and $P_{O_2} = 9.2 \times 10^{-6}$ atm (marked as A). Fig. 8 shows a schematic diagram of the mechanism of zircon reduction under vacuum: zircon on the surface decomposes forming ZrO_2 and SiO_2, and the later volatilizes, decomposing into $SiO_{(g)}$ and $O_{2(g)}$, and a porous zirconia layer is left on the surface.

The relative stabilities of the oxides are studied with the corresponding volatility diagrams. The volatility diagrams of ZrO_2 and Y_2O_3 are shown in Figs. 9 and 10. According to these diagrams, the main reactions the two oxides undergo in the conditions of the experiment are the following:

$$Y_2O_3 \rightarrow 2YO_{(g)} + \tfrac{1}{2}O_{2(g)} \quad (2)$$

$$ZrO_2 \rightarrow ZrO_{2(g)} \quad (3)$$

The equilibrium conditions at 1400 °C and 1×10^{-3} atm of reactions (1)–(3) are read in the isomolar points of the volatility diagrams in Figs. 7, 9 and 10 (labelled A in each of them). The isomolar points are the points of intersection of the isomolar line

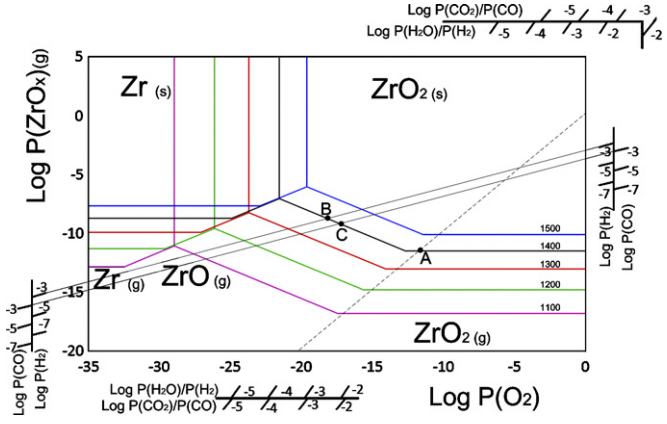

Fig. 9. Volatility diagram for zirconia under a total pressure of 10^{-3} atm and different temperatures.

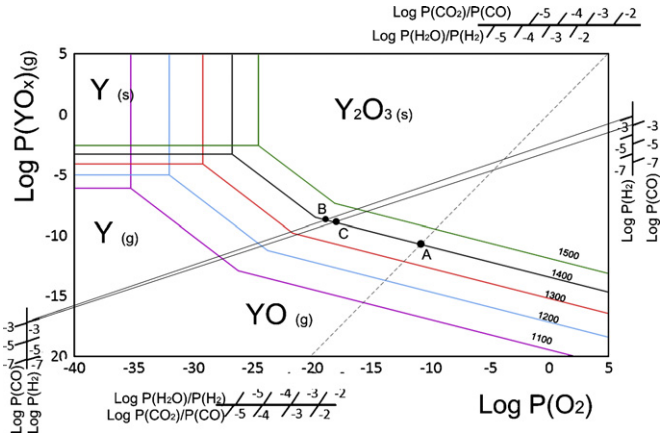

Fig. 10. Volatility diagram for yttria under a total pressure of 10^{-3} atm and different temperatures.

with a maximum equilibrium partial pressure line and define the maximum pressures reached for gaseous species in atmospheres with low P_{O_2}. The volatilization of yttria will produce maximum equilibrium partial pressures of $P_{YO} = 2.4 \times 10^{-11}$ atm and $P_{O_2} = 6.1 \times 10^{-12}$ atm (Fig. 10, point A). On the other hand, zirconia volatilizes mainly as $ZrO_{2(g)}$, the maximum equilibrium partial pressure being $P_{ZrO_2} = 3.6 \times 10^{-12}$ atm independently from P_{O_2} (Fig. 9, point A).

Equilibrium pressures reached in the volatilization of ZrO_2 and Y_2O_3 are below those attained in the volatilization of the $ZrSiO_4$. According to the volatility diagrams, the maximum equilibrium pressure of $SiO_{(g)}$ is considerably higher than those of $YO_{(g)}$ and $ZrO_{2(g)}$ (P_{YO} is around 5×10^7 times lower and P_{ZrO_2} is around 8×10^8 times lower than P_{SiO} under the same conditions). The stability difference between the silica and the other two oxides makes reactions (2) and (3) almost negligible when compared to silica volatilization. Therefore, when SiO_2 is volatilized (as $SiO_{(g)}$ and $O_{2(g)}$), ZrO_2 and Y_2O_3 remain in solid state, practically unaltered, in the form of a porous layer.

The weight losses at different temperatures (as is shown in Fig. 5), are also determined by the thermodynamic equilibrium constants from which the volatility diagrams are constructed. Thus, the maximum equilibrium partial pressure of $SiO_{(g)}$, which at 1400 °C is 1.8×10^{-5}, drops at 1300 °C to 1.5×10^{-6} (labelled T in Fig. 7), 12 times lower, being the reaction much more favoured at higher temperatures.

For longer reaction times, the weight loss rate turned slower (shown by the reduction of the slope of the lines in Fig. 5). This is related to the formation of the stabilized zirconia coating on the surface, which grows in thickness with time, having the effect of a physical barrier to the gases produced in reaction (1) and therefore slowing the volatilization until it practically stops.

The formation of coatings can be extended to other reducing atmospheres, such as $CO_{(g)}$ or $H_{2(g)}$. The same way as under vacuum, the reaction conditions are inferred from the volatility diagrams of the involved chemical species. The reactions taking place on zircon would be the following:

$$ZrSiO_{4(s)} + Y_2O_3 + H_{2(g)} \rightarrow$$

$$ZrO_{2(s)} + Y_2O_3 + SiO_{(g)} + H_2O_{(g)} \quad (4)$$

Table 2
Maximum equilibrium pressures at 1400 °C and total pressure 10^{-3} atm in different atmospheres

Atmosphere	$SiO_{(g)}$ on $ZrSiO_4$ (atm)	$ZrO_{(g)}/ZrO_{2(g)}$ on ZrO_2 (atm)	$YO_{(g)}$ on Y_2O_3 (atm)
Vacuum ($P_{O_2}\downarrow\downarrow\downarrow$)	1.8×10^{-5}	3.56×10^{-12} (ZrO_2)	2.44×10^{-11}
H_2	3.42×10^{-4}	1.85×10^{-9} (ZrO)	1.84×10^{-9}
CO	1.90×10^{-4}	1.03×10^{-9} (ZrO)	1.24×10^{-9}

$$ZrSiO_{4(s)} + Y_2O_3 + CO_{(g)} \rightarrow$$
$$ZrO_{2(s)} + Y_2O_3 + SiO_{(g)} + CO_{2(g)} \quad (5)$$

The intersection points between the isobar lines (read on the nomographs, and corresponding to the partial pressure of the reducing gas) and the equilibrium maximum pressure lines show the maximum partial pressures in equilibrium conditions. For instance, for zircon at 1400 °C and a total pressure of 10^{-3} atm, in H_2 atmosphere ($\log(P_{H_2}) = -3$), the maximum reachable $SiO_{(g)}$ pressure is 3.42×10^{-4} atm (Fig. 7, labelled B), whilst in CO atmosphere ($\log(P_{CO}) = -3$) the maximum equilibrium pressure is 1.90×10^{-4} atm (Fig. 7, labelled C). Hence, using a reducing agent, such as H_2 or CO, the maximum equilibrium partial pressure P_{SiO} is, respectively, 10^5 and 10^4 times higher than under vacuum, thus being the volatilization more favoured.

Under vacuum (reaction (1)), in H_2 atmosphere (reaction (4)) or in CO (reaction (5)), the volatilisation of $ZrSiO_4/Y_2O_3$ samples will generate a porous layer of yttria stabilized zirconia on the surface of the test samples. According to the volatility diagrams of ZrO_2 and Y_2O_3 (Figs. 9 and 10, respectively), the main reactions taking place in these conditions would be the following:

$$Y_2O_{3(s)} + H_{2(g)} \rightarrow 2YO_{(g)} + H_2O_{(g)} \quad (6)$$

$$Y_2O_{3(s)} + CO_{(g)} \rightarrow 2YO_{(g)} + CO_{2(g)} \quad (7)$$

$$ZrO_{2(s)} + H_{2(g)} \rightarrow ZrO_{(g)} + H_2O_{(g)} \quad (8)$$

$$ZrO_{2(s)} + H_{2(g)} \rightarrow ZrO_{(g)} + H_2O_{(g)} \quad (9)$$

The equilibrium pressures H_2 and CO environments are, respectively, 1.84×10^{-9} and 1.24×10^{-9} for $YO_{(g)}$ (Fig. 10, dots B and C), and 1.85×10^{-9} and 1.03×10^{-9} for $ZrO_{2(g)}$ (Fig. 9, dots B and C). The equilibrium partial vapour pressures of both oxides in H_2 and CO atmospheres are about 10^5 times less than those of $SiO_{(g)}$ in the same conditions. Hence, in the same way as in volatilisation at low P_{O_2}, both ZrO_2 and Y_2O_3 will experience practically no volatilization at all compared to silica, remaining as a porous yttria stabilized zirconia layer on the surface of the zircon substrate.

It must be noted there is a change in the volatilization mechanism of ZrO_2: whilst in low P_{O_2} conditions $ZrO_{2(g)}$ is the main gaseous species produced, in the presence of reducing gases, the $ZrO_{(g)}$ species predominates, as the corresponding isobar intersects the $ZrO_{2(s)}$–$ZrO_{(g)}$ equilibrium line.

The maximum vapour pressures are higher when the reaction is held in a reducing atmosphere, in such a way that, under the same total pressure and temperature conditions, zircon will be less stable when using reducing gases, favouring the formation of the porous layer.

This can be seen in Fig. 6. The less purged the furnace is, the higher the weight losses are. This is due to the higher initial concentration of CO. With the experimental setting used, it was not considered safe to work with H_2 or CO atmospheres, Fig. 6 shows how the presence of higher amounts of CO leads to a higher weight loss, due to the change in the maximal equilibrium partial pressure. Read in the volatility diagram for $ZrSiO_4$ (Fig. 7), under a CO pressure of 4×10^{-4} atm, the maximum $SiO_{(g)}$ equilibrium pressure is 1.2×10^{-4} atm, higher than that under vacuum (1.8×10^{-5} atm). In this case, however, the atmosphere of the furnace is not expected to have a constant composition throughout the reaction time, as the amount of CO is not controlled, so the results are qualitative, but enough to realize that the presence of reducing gases increases the weight loss as a result of the change in equilibrium.

Equilibrium pressures on ZrO_2 and Y_2O_3 increase in reducing atmosphere conditions, but those pressures in these conditions are still much lower than that of $SiO_{(g)}$. As a result, zirconia and yttria volatilization will still be non-significant reactions compared to the volatilization of silica. Equilibrium pressures at 1400 °C are compared in Table 2, which shows the equilibrium maximum partial pressures of the oxides present in the system in different atmospheres.

5. Conclusions

Thermal treatments have been carried out on zircon/yttria discs (containing an 8 mol% of Y_2O_3) under low P_{O_2} atmospheres at 1300 and 1400 °C for times ranging between 1 and 4 h. Porous yttria stabilized zirconia coatings (up to 240 μm in thickness) were formed on the discs as a result of this thermal treatment, due to the volatilization of silica as $SiO_{(g)}$ and $O_{2(g)}$. The measured weight losses in the discs and the thickness of the resulting coatings show that the zircon volatilization rate depends on the temperature and duration of the thermal treatments.

The experimental results are consistent with the thermodynamic data in the volatility diagrams of the three oxides forming the system (yttria, silica and zirconia). From these diagrams, it is deduced that the zircon volatilizes with the emission of $SiO_{(g)}$ and $O_{2(g)}$, whilst the two more stable oxides, zirconia and yttria, remain on the surface of the test samples. The amount of yttria added to the zircon in the original mixture, as well as the high temperature conditions led to the stabilization of zirconia, mostly in its cubic form.

Volatility diagrams are also useful when working with different atmospheres, such as H_2 or CO, as they also provide

important thermodynamic information under these circumstances.

Potential applications of the described zirconia coated zircon include electrodes for solid oxide fuel cells (SOFC). The most usual fabrication processes for the obtention of Ni-YSZ anodes is the sintering YSZ and NiO, together with pore-forming particles, such as graphite, being the most extended coating processes tape casting and screen printing. Using the method described in this article would spare the layer forming process, and would be followed by impregnation of the porous layer with conductive material and a catalyst, as described by other authors.[12]

Further work is currently underway, focusing on increasing the homogeneity of zirconia stabilization and reaching a higher control on the pore formation through process variables.

References

1. Stevens, R., *An Introduction to Zirconia* (*2nd ed.*). Magnesium Elektron Ltd., Twickenham, 2000, pp. 12–17.
2. Lewis, G., Applications for traditional ceramics. In *Engineered Materials Handbook, Ceramics and Glasses, Vol. 4*, ed. S. J. Schneider. ASM International, Metals Park, 1991, pp. 893–909.
3. Stinton, D. P., Besmann, T. M., Lowden, R. A. and Sheldon, B. W., Vapor deposition. In *Engineered Materials Handbook, Vol. 4, Ceramics and Glasses*, ed. S.J. Schneider. ASM international, 1991, pp. 215–222.
4. Chen, H. and Ding, C. X., Nanostructured zirconia coating prepared by atmospheric plasma spraying. *Surf. Coat. Technol.*, 2002, **150**(1), 31–36.
5. Geiger, G., Ceramic coatings. *Am. Ceram. Soc. Bull.*, 1992, **71**(10), 1470–1481.
6. Gardner, R. A. and Buchanan, R. C., High temperature loss of silica from zircon and refractory silicates. *J. Electrochem. Soc.*, 1975, **122**(2), 205–210.
7. Lou, L. K., Mitchell, T. E. and Heuer, A. H., Review–graphical displays of the thermodynamics of high-temperature gas–solid reactions and their application to oxidation of metals and evaporation of oxides. *J. Am. Ceram. Soc.*, 1985, **68**(2), 39–58.
8. Rey, P., Souto, A., Santos, C. and Guitián, F., Development of porous corundum layers on cordierite ceramics. *J. Eur. Ceram. Soc.*, 2003, **23**, 2983–2986.
9. Souto, A. and Guitián, F., Novel method for obtaining corundum layers of high surface area on ceramic supports for high-temperature catalysis. *J. Am. Ceram. Soc.*, 2002, **85**(7), 1823–1826.
10. Zaykoski, J., Talmy, I. and Norr, M., Desiliconization of mullite felt. *J. Am. Ceram. Soc.*, 1991, **74**(10), 2419–2427.
11. Bale, C. W., Chartrand, P., Degterov, S. A., Ben Mahfoud, R., Melançon, J., Pelton, A. D. *et al.*, FactSage thermochemical software and databases. *Calphad*, 2002, **26**(2), 189–228.
12. Yamahara, K., Jacobson, C. P., Visco, S. J. and De Jonghe, L. C., Catalyst-infiltrated supporting cathode for thin-film SOFCs. *Solid State Ionics*, 2005, **176**, 451–456.